

Population synthesis on high-mass X-ray binaries: prospects and constraints from the universal X-ray luminosity function

Zhao-Yu Zuo^{1,3}, Xiang-Dong Li^{2,3} and Qiu-Sheng Gu^{2,3}

¹Department of Physics, School of Science, Xi'an Jiaotong University, Xi'an 710049, China

²Department of Astronomy, Nanjing University, Nanjing 210093, China;

³Key laboratory of Modern Astronomy and Astrophysics (Nanjing University), Ministry of Education, Nanjing 210093, China

zuozyu@mail.xjtu.edu.cn; lixd@nju.edu.cn

Received _____; accepted _____

ABSTRACT

Using an updated population synthesis code initially developed by Hurley et al. we modeled the synthetic X-ray binary (XRB) populations for direct comparison with the universal, featureless X-ray luminosity function (XLF) of high mass X-ray binaries (HMXBs) in star-forming galaxies. Our main goal is to use the universal XLF to constrain the model parameters, given the current knowledge of binary evolution. We find that the one-dimensional (1D) Maxwellian velocity dispersion of the natal kick can be constrained to be of the order of $\sigma_{\text{kick}} \sim 150 \text{ km s}^{-1}$, supporting earlier findings that neutron stars (NSs) formed in binaries seem to receive significantly smaller natal kicks than the velocities of Galactic single pulsars would indicate. The super-Eddington accretion factor is further confirmed in the framework of stellar mass black holes (BHs), revealing the true origin of the most of the ultraluminous X-ray sources (ULXs) may indeed be the high-luminosity extension of ordinary HMXBs which harbor stellar-mass BHs rather than exotic intermediate-mass BHs or ones. We present the detail properties of the model-predicted present-day HMXBs, which may be investigated by future high-resolution X-ray and optical observations of sources in nearby star-forming galaxies.

Subject headings: binaries: close - galaxies: evolution - galaxies: general - stars: evolution - X-rays: galaxies - X-ray: binaries - X-rays: stars

1. Introduction

High mass X-ray binaries (HMXBs) are binary systems, in which a high mass primary star formed the compact star accreting from a secondary massive star. They are conventionally divided into two subgroups (van Paradijs 1983). One group usually contains an evolved (super)giant star, generally $M_{\text{opt}} \gtrsim 10M_{\odot}$, having strong stellar wind or filling its Roche lobe (RL) to power a bright X-ray source for $\sim 10^5 - 10^6$ yr. The compact star should be either a neutron star (NS; $M \sim 1.4M_{\odot}$) or a stellar-mass black hole (BH; $\sim 3 < M/M_{\odot} < \sim 20$ for solar metallicity, but may reach ~ 100 in metal-poor environments, see Remillard & McClintock 2006, for reviews) as a result of collapse of high mass primary star. Another possible type of accreting objects may be intermediate-mass ($\sim 10^2 \leq M/M_{\odot} \leq 10^5$) BH (i.e., IMBHs, see van der Marel 2004, for a review), however its exact origin is still not well understood. The other group is so-called Be/X-ray binaries (Be-XRBs), in which it contains a Be (B-type star which shows emission-line spectra) companion, usually accreted by an NS during its periastron passage, showing as X-ray transients.

With Chandra’s unprecedented sensitivity and angular resolution (Weisskopf et al. 2000), a large number of HMXBs have been discovered in galaxies even beyond the Local Group (Fabbiano 2006), allowing to do studies of the collective properties of HMXB populations as a whole. One of the most striking features of HMXB populations is that the X-ray luminosity function (XLF) takes a possibly universal form of a single, smooth power law giving an excellent account of HMXBs containing NSs, stellar-mass BHs and probably IMBHs over the entire X-ray luminosity range $\sim 10^{35} \leq L_X \leq 10^{40} \text{ergs s}^{-1}$. This is first discovered by Grimm, Gilfanov & Sunyaev (2003a), based on *Chandra* and *ASCA* data of nearby star-forming galaxies and *RXTE/ASM*, *ASCA*, and *MIR-KVANT/TTM* observations of our Galaxy and the Magellanic Clouds. They showed that for a wide

range of star formation rate (SFR), the HMXB XLF in a galaxy can be well described by a power law with slope of ~ 1.6 , the normalization of which is proportional to the SFR. They searched for but found no features corresponding to the Eddington luminosities of NS and BH in the averaged XLF. They argued, however, that the expected features may be smeared and diluted by various effects such as distance uncertainties. With a larger sample of galaxies and better control of systematic effects, Mineo, Gilfanov & Sunyaev (2012, hereafter MGS for short) revisited this problem and found that the average HMXB XLF is entirely consistent with the one obtained by Grimm, Gilfanov & Sunyaev (2003a). The accuracy of XLF slope has been improved to ~ 0.03 , and the values of the high luminosity break at $L_X \sim 10^{40} \text{ ergs s}^{-1}$ are consistent within statistical uncertainties. They did not find any statistically significant feature in the XLF near the critical Eddington luminosity of NSs, either.

Although the absence of features in the HMXB XLF is striking and puzzling, theoretical investigations on this remain limited. Using the fundamental mass-luminosity and mass-radius relations for massive stars, as well as a natural assumption on the power-law initial mass function (IMF; Salpeter IMF or Miller-Scalo IMF) and following a semi-empirical approach, Postnov (2003) noted that the universal XLF can be readily explained by the universal properties of mass transfer rates in HMXBs. Bogomazov & Lipunov (2008), using the “Scenario Machine” code (Lipunov et al. 2009), instead argued that there should be no universal XLF in both observational and theoretical aspects. They suggested that the evolution of binaries and their lifetimes in their X-ray stages should be taken into account in future theoretical modelings. Recently, Bhadkamkar & Ghosh (2012) used a Jacobian transformation method to calculate the XLF and the binary-period distribution of HMXBs in the stellar fields of normal galaxies. Their model XLF can match the observed XLF shape quite closely. They suggested that a future Monte Carlo evolutionary population synthesis (EPS) scheme is promising to obtain more detailed understanding of the formation and

evolution of HMXB populations.

In fact population synthesis studies on the XLF have already been examined and explored extensively in the past decade. Several authors focused on the XLF modeling for individual galaxies, the types of which cover almost the entire galaxy morphological sequence, for example the star forming galaxies (see Belczynski et al. 2004, i.e., NGC 1569), star-burst galaxies (Liu & Li 2007, NGC 4038/4039, the Antennae), and elliptical galaxies (Fragos et al. 2008, 2009, NGC 3379 and NGC 4278). Specifically Linden et al. (2010, 2011) modeled the XLF for HMXBs and Be-XRBs in the Small Magellanic Cloud (SMC). Luo et al. (2012) studied the XLFs of XRB populations in NGC 1291, in both the bulge and ring regions. Additionally Lü et al. (2012) calculated the numbers and birthrates of symbiotic XRBs in the Galaxy. Several authors focused on X-ray/XLF evolution or their numbers of a specific type of galaxies globally, instead. However most of them are based on semi-empirical, semi-analytical approaches, with simplified assumptions adopted on the formation and evolution of XRBs (White & Ghosh 1998; Van Bever & Vanbeveren 2000; Ghosh & White 2001; Wu K. 2001; Piro & Bildsten 2002; Bildsten & Deloye 2004; Revnivtsev et al. 2011; Bhadkamkar & Ghosh 2012, 2013a,b). It is worth noting that the more sophisticated, state-of-the-art EPS simulation has also been explored in this direction. The first attempt was done recently by Zuo & Li (2011) on the cosmic X-ray evolution of XRBs in late-type galaxies, and its dependence on the physical properties of galaxies (e.g., optical luminosity, stellar mass, and mass-to-light ratio), which is followed by Fragos et al. (2013) focusing mainly on the global scaling of emission from XRB populations with star-formation rate and stellar mass, and their evolution with redshifts, by using the Millennium-II simulation as initial conditions. As a series of works following Fragos et al. (2013), another two EPS studies are presented recently. One is by Tremmel et al. (2013) studying on the redshift evolution of the normal galaxy XLF as well as integrated XRB emission from entire galaxies, the other is by Tzanavaris et al. (2013) focusing on modeling

the XLFs in galaxies in the Spitzer Infrared Nearby Galaxy Survey (SINGS).

In the present work, we use a most up-to-date EPS code to model the observed XLF (both the shape and the absolute source number) of HMXBs in star-forming galaxies. We also evaluate the effects of several input parameters such as the IMF of binary stars, the natal kick distribution, common envelop (CE) efficiency and super-Eddington factor (see Sec 2.1 for details) on the results. One particular objective of this study is to use the universal featureless XLF to constrain the model parameters. We also aim to explore the detailed components of HMXB populations, which may help understand the nature of the sources and may be testified by future observations.

This paper is organized as follows. In §2 we describe the population synthesis method and the input physics for X-ray binaries (XRBs) in our model. The calculated results and discussion are presented in §3. Our conclusions are in §4.

2. Models

2.1. Assumptions and input parameters

We calculate the expected numbers for various types of HMXB population using a version of EPS code developed by Hurley et al. (2000, 2002) and updated as described in Liu & Li (2007, see Appendix A in their paper) and Zuo et al. (2008). In the present code, the compact object masses are calculated in a different way than originally suggested by Hurley et al. (2000) and Liu & Li (2007). We use a prescription the same as Fryer et al (2012, i.e., the Rapid supernova mechanism), which can reproduce successfully the mass gap observed in Galactic XRBs when combined with binary evolution (Belczynski et al. 2012). We also allow for the formation of low mass NSs through ECS (Podsiadlowski et al. 2004). The maximum NS mass is assumed to be $2.5 M_{\odot}$, above which BH is assumed to

form. We change the recipes for mass loss of stellar winds by using the metal-dependent fitting formulae given by Vink et al. (2001, see also Belczynski et al. 2010). The wind velocity is difficult to determine accurately, and usually set to be proportional to the escape velocity from the surface of the mass-losing star, as a ratio β_{wind} . The values of β_{wind} must depend on the spectral type of the mass-losing star (Lammers et al. 1995; Kucinkas 1999). We adopt $\beta_{\text{wind}} = 0.125$ (i.e., slow winds) for He-rich stars and extended ($R_{\text{don}} > 900R_{\odot}$) H-rich giants, $\beta_{\text{wind}} = 0.8$ for high-mass ($> 1.4M_{\odot}$) main sequence (MS) stars, and the default value 0.5 for others.

Another two major updates are related to the CE evolution. One (and of the most important improvements recently) is on the CE coefficient, λ , which describes the binding energy of the envelope. We now use a more physical estimate of λ (Xu & Li 2010; Loveridge et al. 2011, see below) rather than the constant value conventionally assumed by most previous studies. The other is on the updated critical mass ratio criterion for CE initiated by Hertzsprung gap (HG) donor stars, recently developed by Shao & Li (2013, private communication, see Appendix A). The values of other parameters are adopted the same as the default ones in Hurley et al. (2002) if not mentioned otherwise.

The HMXBs studied by MGS all reside in nearby star-forming galaxies (see their Table 1 for details). Due to heterogeneous data of these galaxies, the metallicity estimation for each galaxy is still not available, however the rough value is most likely to be around subsolar as a whole (private communication with Mineo S.). So we adopted a fixed subsolar metallicity ($0.5Z_{\odot}$) in our basic model. A lower metal abundance mainly affect stellar wind, making it weaker, so we designed a “WEAK” wind model (i.e., model M8) to test this effect. For star formation, a constant SFR of 50 Myr is assumed in our basic model. In each model, we evolve 10^6 primordial systems¹, all of which are initially binary systems.

¹We also vary the number of the binary systems by a factor of eight, and found no

We set up the same grid of initial parameters (primary mass, secondary mass and orbital separation) as Hurley et al. (2002) did and then evolve each binary. In the following we describe the assumptions and input parameters in our basic model (i.e., model M1, listed in Table 1).

(1) initial parameters

We take the IMF of Kroupa (2001, hereafter KROUPA01, with power law slope of -1.3 in $0.08-0.5M_{\odot}$, and -2.3 in $0.5-80.0M_{\odot}$) for the distribution of the primary mass (M_1). For the secondary’s mass (M_2), a uniform distribution is assumed for the mass ratio M_2/M_1 between 0 and 1. We also adopt a uniform distribution for the logarithm of the orbital separation $\ln a$ (Hurley et al. 2002).

(2) CE evolution

When mass transfer becomes dynamically unstable, a binary may enter a CE phase. An important parameter determining the outcome of the CE is the CE parameter α_{CE} (Paczynski 1976; Iben & Livio 1993). It describes the efficiency of converting orbital energy (E_{orb}) into the kinetic energy, resulting in the ejection of the envelope (M_{env}). We use the standard energy prescription (Webbink 1984; Kiel & Hurley 2006) to compute the outcome of the CE phase.

$$E_{\text{bind}} = \alpha_{\text{CE}} \left[\frac{GM_c M_2}{2a_f} - \frac{GM_c M_2}{2a_i} \right], \quad (1)$$

where G is the gravitational constant, a_i and a_f denote the initial and final orbital separations, respectively; M_c is the helium-core mass of the primary star (M_1); E_{bind} the binding energy of the hydrogen-rich envelope. Conventionally, a so-called envelope-structure parameter, λ , defined by

$$E_{\text{bind}} = -\frac{GM_1 M_{\text{env}}}{R_{L_1} \lambda} \quad (2)$$

significant difference in the final results.

is used to compute the binding energy, where R_{L_1} is the RL radius of the primary star. The parameter λ is often assumed to be a constant value (Hurley et al. 2002; Zuo & Li 2010), however in reality it will vary for stars of different masses and different evolutionary phases, far from constant (Dewi & Tauris 2000; van der Sluys et al. 2006). Recent work by Loveridge et al. (2011) presents accurate analytic prescriptions of the envelope binding energy for giants as a function of basic stellar parameters such as the metallicity, mass, radius, and evolutionary phase of the star. They computed the envelope binding energy E_{bind} by integrating the gravitational and internal energies from the core-envelope boundary to the surface of the star M_s as follows,

$$E_{\text{bind}} = \int_{M_c}^{M_s} (E_{\text{in}} - \frac{Gm}{r(m)}) dm, \quad (3)$$

where E_{in} is the internal energy per unit of mass, containing terms such as the thermal energy of the gas and the radiation energy, but not the recombination energy (for more details, see van der Sluys et al. 2006). Here we adopt Loveridge et al. (2011)’s prescription for CE evolution.

(3) *super-Eddington radiation*

In the literature it is often implicitly assumed that the luminosities of accreting NS/BH binaries were constrained by the critical Eddington limit:

$$L_X \lesssim L_{\text{Edd}} \simeq \frac{4\pi G M_1 m_p c}{\sigma_T} = 1.3 \times 10^{38} \frac{M_1}{M_\odot} \text{ ergs s}^{-1}, \quad (4)$$

where σ_T is the Thomson cross section, m_p is the proton mass and c the velocity of light. However we note that in reality this limit may fail for several systems. One possible example is the recently discovered large population of ultra-luminous X-ray sources (ULXs, non-nuclear point-like sources with isotropic X-ray luminosity exceeding $10^{39} \text{ ergs s}^{-1}$), often associated with star-forming regions (Zezas Georgantopoulos & Ward 1999; Roberts & Warwick 2000; Fabbiano, Zezas & Murray 2001). Its luminosity is even

higher than the Eddington luminosity for a $\sim 10M_{\odot}$ accreting BH. Several different scenarios have been proposed to explain its origin, such as HMXBs powered by stellar mass BHs with anisotropic X-ray emission (“beaming” model, King et al. 2001) or with super-Eddington accretion rate/luminosity (due to photon bubble instability, Begelman 2002) or with a combination of the two mechanisms (King 2008). Accretion binaries with a BH mass of $10^2M_{\odot} < m_{\text{BH}} < 10^5M_{\odot}$ (IMBHs) can also be a possibility, however can hardly account for all the ULXs observed in the galaxies, but only the most luminous sources (with $L_X \gtrsim 10^{41} \text{ erg s}^{-1}$). Here we introduce a parameter η_{Edd} , i.e. “Begelman factor” (Rappaport, Podsiadlowski & Pfahl 2004) to examine the allowed maximum super-Eddington accretion rate if powered by stellar mass BHs. In our basic model, η_{Edd} is adopted as 100 for BH XRBs. We also reduce its value to 80, 50, 30, 10 and 5 (i.e., model M4), to examine its effect. On the other hand, NS accretors seem to provide at most several times the Eddington-limited luminosity (Levine et al. 1991, 1993; Grimm et al. 2003b; Rappaport et al. 2005; Fragos et al. 2008), here we adopt η_{Edd} for NS XRBs as 5 and keep this assumption throughout.

(4) *SN kicks*

At the time of birth NSs and BHs receive a velocity kick due to any asymmetry in the supernova (SN) explosions (Lyne & Lorimer 1994). We assign a Maxwellian kick distribution with a dispersion velocity of $\sigma_{\text{kick}} = 150 \text{ km s}^{-1}$ for newborn NSs in our basic model. For BHs, we scale down the natal kick by multiplying the kick by the fraction of material which does not fall back onto the compact objects. Additionally, BHs formed with small amounts of fall back ($M_{\text{fb}} < 0.2M_{\odot}$) are assumed to receive full kicks. In situations where BHs form silently (without a SN explosion) via direct collapse, we apply no natal kick in our basic model (Fryer et al 2012; Dominik et al. 2012). Moreover, for ECS NSs, no natal kick is assumed since these are weak SN occurring for the lowest stars ($M_{\text{ZAMS}} = 7.6 - 8.3M_{\odot}$, Hurley et al. 2000; Eldridge & Tout 2004a,b; Belczynski et al.

2008).

We also construct several other models by varying the key input parameters, as listed in Table 1.

(1) Variations of the CE parameter can change the orbital separation of the binary considerably, resulting in different outcomes of the final evolution. However a reliable value for α_{CE} is difficult to estimate due to a lack of understanding of the complicated processes involved, although it is adopted extensively from ~ 0.1 to ~ 3.0 (e.g., Taam & Bodenheimer 1989; Tutukov & Yungelson 1993; Podsiadlowski, Rappaport & Han 2003) in the literature. Here we adopt $\alpha_{\text{CE}} = 0.5$ in our basic model and change it to 1.0 (model M2) to examine its effect.

(2) Surveys of M dwarfs within 20 pc from the Sun have indicated that the binary fraction f may be a function of stellar spectral types (Fischer & Marcy 1992). For example, recent works by Lada (2006) and Kobulnicky & Fryer (2007) find that for G stars $f > 0.5$ while $f > 0.6$ for massive O/B stars in the Cygnus OB2 association. So we set $f = 0.5$ in our basic model and modify it to $f = 0.8$ (model M3) for comparison.

(3) Observations show that compact young massive clusters contain more massive stars preferentially (Sternberg 1998; Smith & Gallagher 2001), so we also make use of the IMF of Matteucci & Tornambè (1987, hereafter MT87, with power law slope of -1.3 in $0.08\text{-}1.0M_{\odot}$, but -1.95 in $1.0\text{-}80.0M_{\odot}$, model M6), which is more skewed towards high mass than in KROUPA01. For the mass of the secondary star (M_2), a power-law distribution of $P(q) \propto q^{\alpha}$ is assumed, where $q \equiv M_2/M_1$. We adopt both the conventional choice of flat mass spectrum, i.e., $\alpha = 0$ (our basic model, M1, Mazeh et al. 1992; Goldberg & Mazeh 1994; Shatsky & Tokovinin 2002) and $\alpha = 1$ (model M5), since recent observations are more in accord with “twins” being a general feature of the close binary population (Dalton & Sarazin 1995; Kobulnicky & Fryer 2007).

(4) The kick velocity can affect not only the global velocity of the binary system (Zuo & Li 2010) but also the outcome of the XRB evolution. Though the research on natal SN kicks has already had a long history (Bailes 1989), its functional form of the underlying speed distribution is still poorly constrained. Measurements of proper motions for isolated radio pulsars indicate the typical kick speed is in excess of $\sim 100 - 200 \text{ km s}^{-1}$ (Lyne & Lorimer 1994; Hansen & Phinney 1997; Cordes & Chernoff 1998; Arzoumanian et al. 2002; Hobbs et al. 2005), however recent observation of NSs found in binaries seems to reveal that they receive a smaller natal kick (Pfahl et al. 2002; Belczynski et al. 2010b; Wong et al. 2010; Bodaghee et al. 2012), of the order of 100 km s^{-1} . So we also adopt $\sigma_{\text{kick}} = 265 \text{ km s}^{-1}$ (i.e., model M7, Hobbs et al. 2005), 190 km s^{-1} (Hansen & Phinney 1997), 170 km s^{-1} (Belczynski et al. 2010b), 100 km s^{-1} , and 50 km s^{-1} (Bodaghee et al. 2012) for comparison.

(5) Stellar winds from massive stars show a number of puzzles contrasting observational and theoretical aspects. The two most prominent are the “wind clumping” (e.g., Osterbrock & Flather 1959; Markova et al. 2004; Repolust et al. 2004; Lépine & Moffat 2008) and “weak wind problem” (e.g., Chlebowski & Garmany 1991; Kudritzki et al. 1991; Herrero et al. 2002). The former is related to the fact that mass loss rates might be twice overestimated since stellar winds might be forming dense clumps rather than being distributed uniformly. The latter suggests that wind mass loss rates from late O and early B type stars reveal a severe drop, by a factor of ~ 100 than theoretically predicted. Based on this we reduce the wind mass loss rates by a factor of 2 to examine its effects (e.g., weak winds, model M8). This is done for all stars at all points in their nuclear evolution.

2.2. X-ray luminosity and source type

For super-giant/main-sequence (SG/MS) HMXBs we use the same methods to compute the 0.5 – 8 keV X-ray luminosities and divide types of different sources as in Zuo & Li (2011). Accreting NS/BH in XRBs are powered by either disk fed by RLOF or stellar wind. When a star expands to fill its RL, a disk may form transferring masses to the compact star. Otherwise, wind accretion is needed to power an observable X-ray source. For wind accretion, we explore the classical Bondi & Hoyle (1944)’s formula to calculate the mass transfer rate to the compact star. In the RLOF case, we discriminate transient and persistent sources using the criteria of Lasota (2001, i.e., Eq 36 therein) for MS and red giant stars, and of Ivanova & Kalogera (2006, i.e., Eqs 20 and 24 therein) for white dwarf (WD) donors, respectively. For transient systems, the duty cycle (DC) is empirically thought to be less than $\sim 1\%$ (Taam et al. 2000). We adopt DC=1% (probability of finding a system in outburst) in our calculations. The corresponding X-ray luminosity form is as follows:

$$L_{X,0.5-8\text{keV}} = \begin{cases} \eta_{\text{bol}}\eta_{\text{out}}L_{\text{Edd}} & \text{transients in outbursts,} \\ \eta_{\text{bol}} \min(L_{\text{bol}}, \eta_{\text{Edd}}L_{\text{Edd}}) & \text{persistent systems,} \end{cases} \quad (5)$$

where the bolometric luminosity $L_{\text{bol}} \simeq 0.1\dot{M}_{\text{acc}}c^2$ (where \dot{M}_{acc} is the average mass accretion rate), η_{bol} the bolometric correction factor converting the bolometric luminosity (L_{bol}) to the 0.5 – 8 keV X-ray luminosity (Belczynski et al. 2004), adopted as 0.4 though its range is $\sim 0.1-0.5$ for different types of XRB. η_{Edd} is the ‘Begelman’ factor to allow super-Eddington luminosities, as stated above. For transient sources the outburst luminosity is taken as a fraction (η_{out}) of the critical Eddington luminosity. We take $\eta_{\text{out}} = 0.1$ for NS transients and $\eta_{\text{out}} = 1$ for BH transients with orbital period P_{orb} less and longer than 1 day and 10 hr, respectively (Chen et al. 1997; Garcia et al. 2003; Belczynski et al. 2008).

We adopt a phenomenological way to define Be-XRBs as in Belczynski & Ziolkowski

(2009). A HMXB is recognized as Be-XRB if: (1) it hosts NS accretors. We do not consider BH Be-XRBs since no such system has been found so far (Liu et al. 2005, 2006); (2) the donor should be massive ($M_{\text{donor}} \geq 3.0M_{\odot}$) MS star (i.e., O/B star with burning H in its core); (3) accretion proceeds only via stellar wind (no RLOF); (4) only systems with orbital period in the range of 10-300 days are considered; (5) only a fraction $f_{\text{Be}} = 0.25$ of the above systems are designated as hosting a Be star, as this seems to be the fraction of Be stars among all regular B-type stars ($\sim 1/5 - 1/3$, Slettebak 1988; Ziolkowski 2002; McSwain & Gies 2005). So technically, we randomly selected only 25% ($f_{\text{Be}} = 0.25$) of the massive binaries hosting a B/O star to predict their numbers in our EPS calculations. The X-ray luminosities of Be-XRBs are estimated based on its orbital periods using Eq. 11 presented by Dai et al. (2006), the formula of which is obtained by fitting the observed data for 36 Be-XRBs compiled by Raguzova & Popov (2005). For Be transients, the outbursts are short-lived, typically covering a relatively small fraction of the orbital period ($\sim 0.2 - 0.3P_{\text{orb}}$, Reig 2011). Here we adopt an upper value $DC_{\text{max}} = 0.3$ to give the expected maximum source numbers.

3. Results and Discussion

Based on a population of ~ 700 compact sources, MGS constructed the average XLF of HMXBs in galaxies. The HMXB XLF they derived follows a power law with a slope of 1.6 in the broad luminosity range $\log L_X \sim 35 - 40$ and shows a moderately significant evidence for a luminosity break or cut-off at $\log L_X \approx 40$. In addition, they did not find any significant features at the Eddington limit for NS or a stellar mass BH. Moreover when compared with each individual galaxy in their primary sample, which is normalized to their respective SFRs, there are still considerable dispersions in the amplitude (i.e., total number of HMXBs per unit SFR). Here we modeled the HMXB XLF from a theoretical point of

view. The results are presented below.

3.1. Comparison with Mineo, Gilfanov & Sunyaev (2012) and model predictions

We adopted several models with different assumptions for the input parameters (see Table 1). Specifically the input parameters in our basic model (i.e., model M1) are SFH= 50 Myr, $\alpha = 0$, $\alpha_{\text{CE}} = 0.5$, $\eta_{\text{Edd}} = 100$, $f = 0.5$ and the KROUPA01 IMF, while other models are designed by changing only one parameter each time to test its effect. Fig. 1 shows the simulated cumulative XLF and its detailed components contributed by accreting NS/BH with hydrogen-rich (NS/BH-H) and helium-rich (NS/BH-He) MS/SG donors, and Be-XRBs (left panel) and accretion modes of simulated XRBs (right panel), respectively. Note that our simulated XLF can match the observed average XLF pretty well. One can see that BH-H systems dominate the XLF of both the very high luminosity ($L_X > \sim 2 \times 10^{38} \text{ergs s}^{-1}$) and low luminosity ($L_X < 10^{36} \text{ergs s}^{-1}$) end, while NS-H systems play a major role in the luminosity range of $\sim 10^{37} - \sim 10^{38} \text{ergs s}^{-1}$. Moreover they are mainly persistent sources (the transients are very rare). Our calculation shows that the BH-H ULX systems are contributed mainly by two species. They are all persistent sources, the majority of which are mainly wind-fed BH-XRBs with massive ($\sim 10 - 30 M_{\odot}$) SG donors (i.e., BH-SG HMXBs), whose orbital period is in the range of several thousands days to even hundreds of years, with a nearly flat eccentricity distributed from 0 to 1. The other specy is mainly RLOF-fed BH-XRBs, with less massive (typically $< 10 M_{\odot}$) MS donors, whose orbital period is much shorter, typically on the order of days. While BH XRBs at the low luminosity end are mainly wind-fed BH systems powered by higher mass ($\sim 30 - 75 M_{\odot}$) MS stars (i.e., BH-MS HMXBs), with orbital period from about months to $\sim 10^3$ days, as shown in Fig. 2 for the current orbital period $P_{\text{orb}} - L_X$ (left) and $P_{\text{orb}} - M_2$ (right) distribution, respectively. In

addition, the Be-XRB population is predicted to be very small. It is mainly due to the low duty cycle transient characters of Be-XRBs relative to the long-term average of observed XLF, supporting the expectation by Bhadkamkar & Ghosh (2012).

We note that, quantitatively, our calculation is in general consistent with current HMXB population statistics. Our prediction that XRBs with luminosity larger than $\sim 10^{37} \text{ergs s}^{-1}$ are mainly NS systems is in general consistent with observational statistics by Liu et al. (2006). The most luminous sources (for example ULXs) are predicted to be BH systems, which is also not in contradiction with current observation and theoretical expectations. The prediction that HMXB with naked He donor stars is relatively less than HMXB containing H-rich donors is also not at odds with current observational statistics (one He-HMXB confirmed in the Galaxy, i.e., Cyg X-3, van Kerkwijk et al. 1992, and another two extragalactic He-HMXBs IC10 X-1 and NGC300 X-1 confirmed by Crowther et al. 2003, 2010). The predicted ULX HMXBs usually have massive ($\sim 10 - 30 M_{\odot}$) donor stars, accreted by BHs in its SG phase, or less massive ($< \sim 10 M_{\odot}$) MS donors accreted by BH in RLOF phase, which are very similar to the sources identified by Liu et al. (2002, i.e., NGC 3031 X-11), Roberts et al. (2001) and Liu et al. (2004, i.e., ULX in NGC 5204), Zampieri et al. (2004, i.e., NGC 1313 X-2), and Soria et al. (2005, i.e., NGC 4559 X-7). We also predict a preponderance of wind-fed BH HMXBs powered by massive MS stars in relative low luminosities ($L_X < \sim 10^{36} \text{ergs s}^{-1}$) which has not yet been uncovered in nearby star-forming galaxies. Future high resolution X-ray and optical observations of this population may be used as a further test of the results obtained here.

To illustrate the formation and evolution of these BH HMXBs in detail, we present two example evolutionary sequences for M_1 , M_2 , P_{orb} , L_X of BH-SG and BH-MS HMXBs in Figures 3 and 4, respectively. In Fig. 3, we consider a primordial binary system in a $2505.4 R_{\odot}$ circular orbit. The initial stellar masses are 30.119 and $27.158 M_{\odot}$ for the

primary and secondary, respectively. The primary first evolves across the HG, expands and fills its RL in the core helium burning (CHeB) stage (time 6.3257 Myr), then transfers mass to the secondary star, which is still on the MS. As mass transfer proceeds the orbit of the system first shrinks slightly then expands to $\sim 2995.244 R_{\odot}$ as the mass ratio gets flipped at the time of 6.5931 Myr until the binary gets detached again (time 6.9195 Myr). As the binary evolves the orbit of the system expands slightly until the time of 7.0079 Myr when the primary forms a BH (the CO core mass $M_{\text{CO}} = 7.9972 M_{\odot}$, hence partial fall-back with reduced natal kicks), the orbital separation of which is sharply increased to $\sim 5340.816 R_{\odot}$ with a large eccentricity of ~ 0.46 . At this time, the system consists of a $6.50 M_{\odot}$ BH and a massive ($M_2 = 37.181 M_{\odot}$) MS companion. Then the rejuvenated MS star, as the primary, evolves across the HG, expanding its radius to become a SG star at the time of ~ 7.78 Myr. At this time the SG donor which has extremely large radii ($> 1000 R_{\odot}$) has sufficiently strong stellar winds to power a bright HMXB activity before SN explosion which results in another BH and the disruption of the binary system.

Next, we use a binary with initially $M_1 = 39.816 M_{\odot}$, $M_2 = 22.178 M_{\odot}$ and $a = 62.743 R_{\odot}$, to give a quick illustration of BH-MS HMXB formation and evolution, as shown in Fig. 4. The primary fills its RL on its MS, and mass transfer proceeds as it evolves across HG till the end of CHeB, at which point (time 5.1369 Myr) it is a $12.632 M_{\odot}$ naked HeMS star in a $a = 124.107 R_{\odot}$ orbit with a $45.730 M_{\odot}$ MS companion. Then the HeMS star evolves across the HeHG, and explodes at the time of 5.7680 Myr, leaving a $5.497 M_{\odot}$ BH with a $45.327 M_{\odot}$ MS companion in an orbit of $163.7139 R_{\odot}$. The strong stellar wind from the MS star is then accreted by the BH at a moderately low rate compared with the SG case above, resulting in relatively low luminosity BH-MS XRBs powered by stellar wind. As the MS star evolves across the HG and fills its RL, the BH will spiral into its envelope due to the extremely large mass ratio, leading to a coalescence finally at the time of 8.4605 Myr, immediately after entering the CE phase.

We note that the above evolutionary sequence example may explain why BH binaries with massive MS donors can dominate at lower luminosities, rather than binaries with NS accretors. It is mainly because of the fact that the SN kicks the compact stars receive during SN explosion are quite different. As illustrated above, the BH in BH-MS HMXB always receives a small or no SN kick, which facilitates the survival of a wide binary, which would probably produce a faint HMXB. However it is not the case for NSs. Due to the much larger SN kicks, the NS is more likely to escape from its companion, leading to the disruption of the binary system. Or if survived luckily it may expand its orbit greatly, showing likely as Be/X-ray transients when active. However even so, such a channel is still insignificant when compared with BH-MS HMXBs, as already estimated.

In Fig. 5, we show the evolution of XLF in our basic model, in order to study the nature of the sources, as well as its evolution. Both constant star formation (left) and a δ -function like star formation (right) cases are studied. We note that most of the sources are produced within ~ 20 Myr after the star formation, which is in general agreement with observations (Swartz et al. 2009) and previous studies (Linden et al. 2010). We suggest that the short formation and lived time scale of sources may explain why the universal XLF should exist naturally in the star-forming galaxies. Additionally we see that the more recent star formation seems to have more luminous sources, resulting in a much flatter XLF at the high luminosity end. Our results are consistent with earlier observations (see Fabbiano 2006, and references therein), revealing that the different or more complex XLFs are mainly because of the complexity and evolution of the X-ray source populations. Moreover the BH-MS HMXBs seem to emerge a little earlier than BH-SG HMXBs. This can be understood when considering the fact that the sources in both luminosity extremes have distinct formation channels. As illustrated above, we can see that the appearance of BH-MS sources always accompanies with the birth of the BH accretors, the progenitors of which have a shorter nuclear evolution timescale when compared to the BH-SG HMXBs,

the occurrence of which while is mainly driven by the expanding of the less massive donor stars. However the SG donors have always much stronger stellar winds than MS stars, leading to much brighter BH-SG HMXBs when compared to BH-MS sources.

3.2. Effects of parameters on XLFs

Fig. 6 shows XLFs for different models compared to our basic model M1 (solid line). Each model is chosen to examine the effect that each parameter has on both the shape and the absolute source number of the XLF. Several parameters have significant effects on either the shape or the source number or both of the XLFs, while others have only minor effects.

The parameters that have minor effects include the CE efficiency parameter (α_{CE}), and the initial mass ratio distribution of the secondary star, as shown by models M2 and M5, respectively. The parameter α_{CE} dictated how efficiently orbital energy is transformed into the kinetic energy that expels the donor’s envelope during the CE phase. It mainly affects the formation and evolution of binary systems which must go through a CE phase, such as low mass X-ray binaries (LMXBs) (Tremmel et al. 2013) and cataclysmic variables (Paczynski 1976). However this is not the case for HMXBs, as the major formation channels of HMXBs do not involve CE phases as severely as LMXBs (Linden et al. 2010; Valsecchi et al. 2010). We also change α_{CE} to other values and forms (for details see Zuo & Li 2013, and comparisons with the γ -algorithm). Changing the initial binary mass ratio from a flat distribution (model M1) to a “twins” distribution (model M5) has little effect on the XLF, although there is a slight increase in the number of bright HMXBs. This is because HMXBs require mass ratios close to one which is achieved by the “twins” model which forces mass ratios close to unity.

The binary fraction only affects the absolute source number of the XLF. As shown

in Fig. 5 an increase of binary fraction (i.e., model M3) means more XRBs are produced, hence an overall shift of the XLF curve compared to that of the basic model. A flatter IMF (i.e., model M6) implies a larger number of massive stars, resulting in more compact objects compared to a steeper one. Hence a flatter IMF will result in more luminous HMXBs.

We suggest that the diversity of stellar components may explain the normalization dispersions of XLFs between galaxies. We note that the simulated star-forming galaxy in our basic model only represents a typical case for this kind of galaxies. While for each individual galaxy, it may have its specific stellar properties, such as different stellar mass distributions (for both the primary and the secondary), and different binary fractions. Our parameter studies (IMF, f and $P(q)$) precisely support the idea that the normalization dispersion is of a physical origin, proposed by MGS. However we emphasize that the intrinsic physics governing the binary evolution should keep the same for binaries in these galaxies, as examined below.

In model M4, a significant luminosity break emerges when decreasing the 'Begelman factor' η_{Edd} by a factor of ~ 20 (dotted line in Figures 6 and 7, respectively). A similar trend has been found previously (Liu & Li 2007; Linden et al. 2010). In order to better constrain the super-Eddington factor, we modify the 'Begelman factor' to 80 (dash-dotted line), 50 (dash-dot-dotted line), 30 (long-dashed line), 10 (short-dashed line), respectively, as shown in Fig. 7. We note the luminosity break exists clearly even for η_{Edd} as high as $\sim 30 - 50$. This marked contrast with the observed smooth XLF implies that the actual maximum luminosities of accreting BHs can be as high as even ~ 100 times the corresponding Eddington luminosities, as suggested by Begelman (2002).

Increasing the dispersion velocity σ_{kick} means that natal kicks of high magnitude are chosen more frequently from the Maxwellian distribution. As a consequence more binaries are disrupted during the SN explosions. This decreases the pool of potential HMXBs and

may account for the smaller number of HMXBs in model M7 (dash-dot-dotted line) as shown in Figures 6 and 8, respectively. Additionally, a larger natal kick can move the wind-fed BH-MS HMXBs into a much wider orbit, too widely separated for stellar material to be effectively accreted onto the BH, resulting in much lower luminosities, and hence a smaller number of BH-MS XRBs in this luminosity range. This phenomenon is shown clearly in Fig. 8 where the dispersion of kick velocity σ_{kick} is modified to 190 (dash-dotted line), 170 (dotted line), 100 (short-dashed line), and 50 (long-dashed line), respectively. We note that compared with our basic model the predicted number of low luminosity HMXBs decreases with increasing natal kicks, while smaller σ_{kick} may increase the formation rate of HMXBs remarkably. Specifically, models with high natal kicks (i.e., model M7) predict significantly less HMXBs than are observed, while models with low natal kicks (i.e., $\sigma_{\text{kick}} < \sim 100 \text{ km s}^{-1}$) predict too many HMXBs. Based on these results, we conclude that our models in which the natal kick velocity dispersion above $\sim 200 \text{ km s}^{-1}$ or below $\sim 100 \text{ km s}^{-1}$ are inconsistent with the observations. The typical kicks that match the observed HMXB XLF are on the order of $\sigma_{\text{kick}} \sim 150 \text{ km s}^{-1}$. Using a similar method Belczynski et al. (2010b) proposed a comparable value of natal kick dispersion ($\sigma_{\text{kick}} \sim 170 \text{ km s}^{-1}$) to match the observed intrinsic ratio of double and single recycled pulsars in the Galactic disc. Our finding is in general consistent with theirs. It is not surprising as isolated recycled pulsars and double neutron star (DNS) binaries are both presumably the descendant of NS HMXBs. Our conclusions may further support earlier findings that NSs formed in binaries receive significantly smaller natal kicks than the velocities of Galactic isolated pulsars would seem to indicate.

Stellar winds play an important role in the evolution of high mass stars in two major competing ways. A stronger stellar wind will increase the accretion rate of wind-fed HMXBs, making it more luminous. On the contrary, a weaker stellar wind will result in a larger pre-SN mass, and hence the formation of more numerous and more massive BHs.

This may increase the luminosities of HMXB populations, as on the one hand, BH-XRBs can form stable RLO XRBs with more massive companions compared to NS-XRBs, and on the other hand, more massive BHs may drive higher accretion rate, and therefore higher luminosities. Comparing models M1 and M8, we can see that weaker stellar winds increase both the number and luminosity of bright HMXBs, so the latter effect is the dominant one. We note here that our findings are also consistent with the results obtained by Fragos et al. (2013) and Tremmel et al. (2013).

Our results are subject to some uncertainties and simplified treatments. For example, in our calculations, only HMXBs with stellar mass BHs are considered. However IMBH which is presumably formed through BH mergers may also show up as ULXs. Though it is expected to be significantly less frequent than stellar mass BHs, we should caution that, even only one of this kind of source may change the high luminosity tail of XLF significantly. A further careful modeling of IMBH considering dynamical formation processes may resolve this problem, however it is beyond the scope of this paper. On the other hand in the framework of stellar mass BHs, we may see that the ULX population can be generally accounted for by normal HMXBs, only in the case of mild super-Eddington accretion rate allowed. Additionally, since little is yet known about, either the detail SFH and IMF in star-forming galaxies, or key processes, such as the detailed accretion modes in XRBs, it is difficult to ascertain which parameter combinations are the best or most realistic by comparison with observations. For example, the normalization of the simulated XLF depends on the adopted values of several parameters, such as the bolometric correction factor η_{bol} and binary fraction f . These two parameters show some degeneracy, and a slightly lower bolometric correction factor would favor a larger binary fraction. However the overall shape of the simulated XLF depends most strongly on two parameters: the natal kick dispersion σ_{kick} and the allowed boost factor of super-Eddington accretion rate η_{Edd} . The former, related to the binary interactions, determines the final outcome of the

SN explosion. The latter is related to the accretion behavior, and constrains the location of the break in the XLF. They jointly determine the shape of the XLF. Conversely, the confirmed universal featureless XLF can make a good decision for the precise choice of the corresponding parameters.

4. SUMMARY

We have used an EPS code to model the universal featureless XLF of HMXBs in star-forming galaxies. We used the apparent universal XLF to constrain models of XRBs. Our study shows that the single, smooth power law XLF can be excellently reproduced with all models considered, but with two parameters strongly affecting its overall shape: the dispersion of natal kick velocity σ_{kick} and the introduced parameter “Begelman factor” η_{Edd} . The overall shape and normalization of HMXB XLF need the natal kick dispersion $\sigma_{\text{kick}} \sim 150 \text{ km s}^{-1}$, which is generally consistent with the finding by Belczynski et al. (2010b) based on the statistics of double and single recycled pulsars. Our XLF modeling further strengthens earlier finding that NSs formed in close interacting binaries receive significantly smaller natal kicks than the velocities of Galactic single pulsars would indicate. The absence of features in the XLF near the critical Eddington luminosity of a NS or a stellar-mass BH and the cut-off luminosity at $L_X \sim 10^{40} \text{ ergs s}^{-1}$ need the allowed boost factor of super-Eddington accretion rate as high as $\sim 80 - 100$. Our results give strong supports for the suggestion by Grimm, Gilfanov & Sunyaev (2003a) that the bulk of ULXs may indeed be the high-luminosity extension of ordinary HMXBs which harbor stellar-mass BHs with mildly super-Eddington accretion rate, rather than exotic intermediate-mass objects. We present the detail components of HMXB populations which contribute to the observed XLF, and emphasize that the low luminosity sources of $L_X < 10^{36} \text{ ergs s}^{-1}$ are mainly wind-fed BH systems powered by high mass ($\sim 30 - 75 M_{\odot}$) MS stars with

orbital periods around months to $\sim 10^3$ days which have not yet been verified in nearby star-forming galaxies due to limited instrument capabilities. Our work motivates further high-resolution X-ray and optical observations of HMXB populations in nearby star-forming galaxies.

We thank Marc van der Sluys for providing routines to compute envelope binding energies of giant stars and helpful discussions. We thank Zhi-Yuan Li for his assistance with the language improvement. This work was supported by the National Natural Science Foundation (grants 11103014, 11133001, 10873008 and 11003005), the Research Fund for the Doctoral Program of Higher Education of China (under grant number 20110201120034), the National Basic Research Program of China (973 Program 2009CB824800), the Fundamental Research Funds for the Central Universities and National High Performance Computing Center (Xi'an).

REFERENCES

- Arzoumanian, Z., Chernoff, D. F., & Cordes, J. M. 2002, *ApJ*, 568, 289
- Bailes, M., 1989, *ApJ*, 342, 917
- Baldry, I. K., & Glazebrook, K. 2003, *ApJ*, 593, 258
- Begelman, M. C., 2002, *ApJ*, 568L, 97
- Belczynski, K., Kalogera, V., Rasio, F. A., Taam, R. E., Zezas, A., Bulik, T., Maccarone, T. J., & Ivanova, N. 2008, *ApJS*, 174, 223
- Belczynski, K., Dalogera A., Zezas A., & Fabbiano, G., 2004, *ApJ*, 601, L147
- Belczynski, K., & Taam, R. E. 2004, *ApJ*, 616, 1159
- Belczynski, K., Bulik, T., Fryer, C., Ruiter, A., Valsecchi, F., Vink, J. S., & Hurley, J. R., 2010a, *ApJ*, 714, 1217
- Belczynski, K., Lorimer, D. R., Ridley, J. P., & Curran, S. J., 2010b, *MNRAS*, 407, 1245
- Belczynski, K., Wiktorowicz, G., Fryer, C. L., Holz, D. E., & Kalogera, V., 2012, *ApJ*, 757, 91
- Belczynski, K., & Ziolkowski, J. 2009, *ApJ*, 707, 870
- Bhadkamkar, H., & Ghosh, P., 2012 *ApJ*, 476, 22
- Bhadkamkar, H., & Ghosh, P. 2013a, *astro-ph/1301.1269*
- Bhadkamkar, H., & Ghosh, P. 2013b, *astro-ph/1301.1283*
- Bildsten, L., & Deloye, C. J. 2004, *ApJ*, 607, 119
- Bodaghee, A., Tomsick, J. A., Rodriguez, J., & Berian James, J. 2012, 744, 108

- Bogomazov, A. I., & Lipunov, V. M. 2008, *Astronomy Reports*, 52, 299
- Bondi, H., & Hoyle, F. 1944, *MNRAS*, 104, 273
- Chen, W., Shrader, C. R., & Livio, M. 1997, *ApJ*, 491, 312
- Chlebowski, T., & Garmany, C. D. 1991, *ApJ*, 368, 241
- Cordes, J. M., & Chernoff, D. F. 1998, *ApJ*, 505, 315
- Crowther, P.A., Drissen, L., Abbott, J.B., Royer, P., Smartt, S.J. 2003, *A&A*, 404, 483
- Crowther, P. A., Barnard, R., Carpano, S., Clark, J. S., Dhillon, V. S., Pollock, A. M. T.
2010, *MNRAS*, 403, 41
- Dalton, W. W., & Sarazin, C. L. 1995, *ApJ*, 448, 369
- Dai, H. L., Liu, X. W. & Li, X. D. 2006, *ApJ*, 653, 1410
- Dewi, J. D. M., & Tauris, T. M., 2000, *A&A*, 360, 1043
- Dominik, M., Belczynski, K., Fryer, C., Holz, D., Berti, E., Bulik, T., Mandel, I., &
O’Shaughnessy R., 2012, *ArXiv e-prints*
- Eldridge, J., & Tout, C., 2004a, *MNRAS*, 348, 201
- Eldridge, J., & Tout, C., 2004b, *MNRAS*, 353, 87
- Fabbiano, G. 2006, *ARA&A*, 44, 323
- Fabbiano, G., Zezas, A., & Murray, S. S., 2001, *ApJ*, 554, 1035
- Fischer, D. A., & Marcy, G. W. 1992, *ApJ*, 396, 178
- Fragos, T., et al., 2008, *ApJ*, 683, 346

Fragos, T., et al., 2009, ApJ, 702, 143

Fragos, T., Lehmer, B., Tremmel, M., Tzanavaris, P., Basu-Zych, A., Belczynski, K.,
Hornschemeier, A., Jenkins, L., Kalogera, V., Ptak, A., & Zezas, A. 2013, ApJ, 764,
41

Fryer, C. L., Belczynski, K., Wiktorowicz, G., Dominik, M., Kalogera, V., & Holz D. E.,
2012, ApJ, 749, 91

Garcia, M. R., Miller, J. M., McClintock, J. E., King, A. R., & Orosz, J. 2003, ApJ, 591,
388

Ghosh, P. & White, N. E. 2001, ApJ, 559, L97

Goldberg, D., & Mazeh, T. 1994, A&A, 282, 801

Grimm, H.-J., Gilfanov, M., & Sunyaev, R., 2003a, MNRAS, 339, 793

Grimm, H., Gilfanov, M., & Sunyaev, R., 2003b, Chin. J. Astron. Astrophys. Suppl., 3, 257

Hansen, B., & Phinney, E., 1997, MNRAS, 291, 569

Herrero, A., Puls, J., & Najarro, F. 2002, A&A, 396, 949

Hobbs, G., Lorimer, D. R., Lyne, A. G., & Kramer, M., 2005, MNRAS, 360, 963

Hurley, J. R., Pols, O. R., & Tout, C. A., 2000, MNRAS, 315, 543

Hurley, J. R., Tout, C. A., & Pols, O. R., 2002, MNRAS, 329, 897

Iben, Jr. I., & Livio, M. 1993, PASP, 105, 1373

Ivanova, N., & Kalogera, V. 2006, ApJ, 636, 985

Kiel, P.D., & Hurley, J.R., 2006, MNRAS, 369, 1152

- King, A. R., Davies, M. B., Ward, M. J., Fabbiano, G., & Elvis, M., 2001, *ApJL*, 552, 109
- King, A. R., 2008, *MNRAS*, 385L, 113
- Kobulnicky, H. A., & Fryer, C. L. 2007, *ApJ*, 670, 747
- Kroupa, P. 2001, *MNRAS*, 322, 231
- Kucinkas, A. 1999, *Ap&SS*, 262, 127
- Kudritzki, R. P., Puls, J., Gabler, R., & Schmitt, J. H. M. M. 1991, in *Extreme Ultraviolet Astronomy*, ed. R. F. Malina & S. Bowyer, 130
- Lada, C. J. 2006, *ApJ*, 640, L63
- Lamers, H. J., Snow, T. P., & Lindholm, D. M., 1995, *ApJ*, 455, 269
- Lasota, J. P. 2001, *New Astronomy Reviews*, 45, 449
- Lépine, S., & Moffat, A. F. J. 2008, *AJ*, 136, 548
- Levine, A., Rappaport, S., Deeter, J. E., Boynton, P. E., & Nagase, F. 1993, *ApJ*, 410, 328
- Levine, A., Rappaport, S., Putney, A., Corbet R., & Nagase F. 1991, *ApJ*, 381, 101
- Linden, T., kalogera, V., Sepinsky, J. F., Prestwich, A., Zezas, A., & Gallagher, J. S. 2010, *The Astrophysical Journal*, 725, 1984
- Linden, T., Sepinsky, J. F., kalogera, V., & Belczynski, K. 2009, *ApJ*, 699, 1573
- Lipunov, V. M., Postnov, K. A., Prokhorov, M. E., & Bogomazov, A. I. 2009, *Astronomy Reports*, 53, 915
- Liu, J. F., Bregman, J.N., Seitzer, P. 2002, *ApJ*, 580, L31
- Liu, J. F., Bregman, J.N., Seitzer, P. 2004, *ApJ*, 602, 249

- Liu, Q. Z., van Paradijs, J., & van den Heuvel, E. P. J. 2005, *A&A*, 442, 1135
- Liu, Q. Z., van Paradijs, J., & van den Heuvel, E. P. J. 2006, *A&A*, 455, 1165
- Liu, X. W., & Li, X. D., 2007, *ChJA&A*, 7, 389
- Loveridge, A. J., van der Sluys, M. V., & Kalogera V., *ApJ*, 2011, 743, 49
- Luo, B., et al. 2012, *ApJ*, 749, 130
- Lü G. L., Zhu, C. H., Postnov, K. A., Yungelson, L. R., Kuranov, A. G., Wang, N., 2012, *MNRAS*, 424, 2265
- Lyne, A. G., & Lorimer, D. R., 1994, *Nature*, 369, 124
- Markova, N., Puls, J., Repolust, T., & Markov, H. 2004, *A&A*, 413, 693
- Matteucci, F., & Tornambè A., 1987, *A&A*, 185, 51
- Mazeh, T., Goldberg, D., Duquennoy, A., & Mayor, M. 1992, *ApJ*, 401, 265
- McSwain, M. V., & Gies, D. R. 2005, *ApJS*, 161, 118
- Mineo S., Gilfanov M., & Sunyaev R., 2012, *MNRAS*, 419, 2095 (MGS)
- Osterbrock, D., & Flather, E. 1959, *ApJ*, 129, 26
- Paczynski B., 1976, in Eggleton P., Mitton S., Whelan J. (eds.) *Structure and Evolution in Close Binary Systems. Proc. IAU Symp. 73*, Reidel, Dordrecht, p. 75
- Pfahl, E., Rappaport, S., Podsiadlowski, P., & Spruit, H., 2002, *ApJ*, 574, 364
- Piro, A. L., & Bildsten, L. 2002, *ApJ*, 571, 103
- Podsiadlowski, P., Rappaport, S. A., & Han, Z. 2003, *MNRAS*, 341, 385

- Podsiadlowski, P., Langer, N., Poelarends, A. J. T., Rappaport, S., Heger, A., & Pfahl, E. 2004, *ApJ*, 612, 1044
- Postnov, K., 2003, *Astr Let*, 29, 372
- Raguzova, N. V., & Popov, S. B. 2005, *Astron. Astrophys. Trans.*, 24, 151
- Rappaport, S. A., Podsiadlowski, P., & Pfahl, E., 2004, *MNRAS*, 361, 971
- Rappaport, S. A., Podsiadlowski, P., & Pfahl, E., 2005, *MNRAS*, 356, 401
- Reig, P. 2011, *Ap&SS*, 332, 1
- Remillard, R.A., & McClintock, J.E. 2006, *ARA&A*, 44, 49
- Repolust, T., Puls, J., & Herrero, A. 2004, *A&A*, 415, 349
- Revnivtsev, M., Postnov, K., Kuranov, A., & Ritter, H. 2011, *A&A*, 526, 94
- Roberts, T. P., Goad, M. R., Ward, M. J., Warwick, R. S., O’Brien, P. T., Lira, P., Hands, A. D. P. 2001, *MNRAS*, 325, L7
- Roberts, T., & Warwick, R., 2000, *MNRAS*, 315, 98
- Shao, Y., & Li, X. D. 2013, in preparation
- Shatsky, N., & Tokovinin, A. 2002, *A&A*, 382, 92
- Slettebak, A. 1988, *PASP*, 100, 770
- Smith, L. J., & Gallagher, J. S. 2001, *MNRAS*, 326, 1027
- Smith, D. A., & Wilson, A. S. 2003, *ApJ*, 591, 138
- Soria, R., Cropper, M., Pakull, M., Mushotzky, R., & Wu, K. 2005, *MNRAS*, 356, 12

- Sternberg, A., 1998 ApJ, 506, 721
- Swartz, D. A., Tennant, A. F., & Soria, R. 2009, ApJ, 703, 159
- Taam, R., & Bodenheimer, P. 1989, ApJ, 337, 849
- Taam, R. E., King, A. R., & Ritter, H. 2000, ApJ, 541, 329
- Tremmel, M., Fragos, T., Lehmer, B. D., Tzanavaris, P., Belczynski, K., Kalogera, V., Basu-Zych, A. R., & Farr W. M., et al., 2013, ApJ, 766, 19
- Tutukov, A. V., & Yungelson, L. R. 1993, MNRAS, 260, 675
- Tzanavaris, P., et al. 2013, ApJ, 774, 136
- Valsecchi, F., Glebbeek, E., Farr, W. M., Fragos, T., Willems, B., Orosz, J. A., Liu, J., & Kalogera, V. 2010, Nature, 468, 77
- Van Bever, J., & Vanbeveren, D. 2000, A&A, 358, 462
- van der Marel R. P., 2004, in Ho L., ed., Coevolution of Black Holes and Galaxies, Cambridge Univ. Press, p. 37
- van der Sluys, M. V., Verbunt F., & Pols O. R., 2006, A&A, 460, 209
- van Kerkwijk, M. H. et al. 1992, Nature, 355, 703
- van Paradijs, J. 1983, in Accretion Driven Stellar X-ray Sources, ed. W. H. G. Lewin, & E. P. J. van den Heuvel, Cambridge, 189
- Vink, J. S., de Koter, A., & Lamers, H. J. G. L. M., 2001, A&A, 369, 574
- Webbink, R.F., 1984, ApJ, 277, 355

- Weisskopf, M.C., Tananbaum, H.D., Van Speybroeck, L.P., & O'Dell S.L., 2000. Proc. SPIE, 4012, 2
- White, N. E. & Ghosh, P. 1998, ApJ, 504, L31
- Wu K., 2001, PASA, 18, 443
- Wong, T.-W., Willems, B., & Kalogera, V. 2010, ApJ, 721, 1689
- Xu, X. J., & Li X. D., 2010, ApJ, 716, 114
- Zampieri, L., Mucciarelli, P., Falomo, R., Kaaret, P., Di Stefano, R., Turolla, R., Chierigato, M., Treves, A. 2004, ApJ, 603, 523
- Zezas, A., Georgantopoulos, I., & Ward, M. J., 1999, MNRAS, 308, 302
- Ziolkowski, J. 2002, MmSAI, 73, 1038
- Zuo, Z. Y., Li, X. D., & Liu, X. W. 2008, MNRAS, 387, 121
- Zuo, Z. Y., & Li, X. D. 2010, MNRAS, 405, 2768
- Zuo, Z. Y., & Li, X. D. 2011, ApJ, 733, 5
- Zuo, Z. Y., & Li, X. D. 2013, in preparation

5. APPENDIX A

Rather than a constant value adopted conventionally, a critical mass ratio q_{cr} determining the allowed parameter space for stable mass transfer in the $P_{\text{orb}} - M_1$ plane is developed recently by Shao & Li (2013). For a specific binary consisting of a massive primary star and a less massive secondary, if P_{orb} is initially too short, the orbital separation will always decrease with mass transfer, a sufficiently dense gas flow may exceed the Roche lobe, leading to a CE phase. On the other hand, if the P_{orb} is too long, the primary may have climbed to the (super)giant branch and developed a deep convective envelope around the compact core prior to mass exchange, a runaway mass transfer will happen, leading to the CE evolution. Thus for each mass ratio q , there exist both upper and lower limits of the orbital period ($P_{\text{orb,up}}$ and $P_{\text{orb,low}}$), between which the binary can evolve smoothly with stable mass transfer on thermal timescale.

Shao & Li (2013) provide two choices of metallicity ($Z = 0.001$ and $Z = 0.02$). In our cases, the higher and more appropriate value, i.e., $Z = 0.02$ is adopted, the grid of which we believe can be used without too much loss in accuracy. The corresponding upper and lower limits of orbital period ($P_{\text{orb,up}}$ and $P_{\text{orb,low}}$) for a certain mass ratio q are fitted as a function of initial primary mass (M_1) in the form of binomial:

$$P_{\text{orb}} = \sum_{n=0}^5 a_n M_1^n$$

coefficients of which are listed in Table 2. The upper part of Table 2 is for lower limits, with eleven discrete values of q in the range of 2 to 12. The upper limits of orbital period for each q are very similar, so we give only one rough fitting, the coefficients of which are listed in the lower part of Table 2 (labeled as 'ALL').

Table 1: Parameters adopted for each model. Here α_{CE} is the CE parameter, q the initial mass ratio, IMF is the initial mass function, f binary fraction, η_{Edd} - the factor of super-Eddington accretion rate allowed, σ_{kick} the dispersion of kick speed, STD is the standard stellar winds while WEAK represents the standard wind mass loss rate reduced to 50%.

Model	α_{CE}	$P(q)$	IMF	f	η_{Edd}	σ_{kick}	winds
M1	0.5	$\propto q^0$	KROUPA01	0.5	100	150	STD
M2	1.0	$\propto q^0$	KROUPA01	0.5	100	150	STD
M3	0.5	$\propto q^0$	KROUPA01	0.8	100	150	STD
M4	0.5	$\propto q^0$	KROUPA01	0.5	5	150	STD
M5	0.5	$\propto q^1$	KROUPA01	0.5	100	150	STD
M6	0.5	$\propto q^0$	MT87	0.5	100	150	STD
M7	0.5	$\propto q^0$	KROUPA01	0.5	100	265	STD
M8	0.5	$\propto q^0$	KROUPA01	0.5	100	150	WEAK

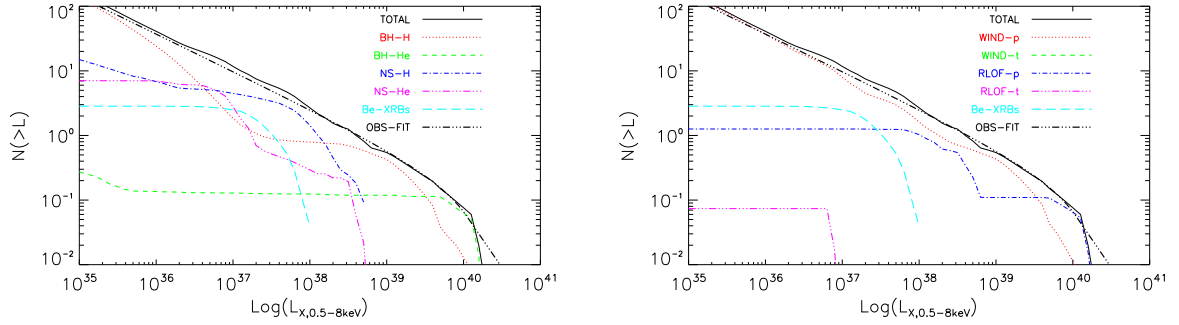


Fig. 1.— The detailed components of the simulated XLF (*left*) and accretion modes of simulated XRBs (*right*) in model M1. *Left* panel: The solid, dotted, short-dashed, dash-dotted, dash-dot-dotted, long-dashed lines represent ALL-XRBs, BH-H, BH-He, NS-H, NS-He MS/SGXRBs and Be-XRBs, respectively. *Right* panel: The solid, dotted, short-dashed, dash-dotted, dash-dot-dotted, long-dashed lines represent ALL-XRBs, wind-fed persistent (WIND-p), wind-fed transient (WIND-t), RLOF-fed persistent (RLOF-p), RLOF-fed transient (RLOF-t) sources and Be-XRBs, respectively. The thick dash-dot-dotted line represents the derived average XLF (labeled as “OBS-FIT”) by MGS using the data of 29 nearby star-forming galaxies.

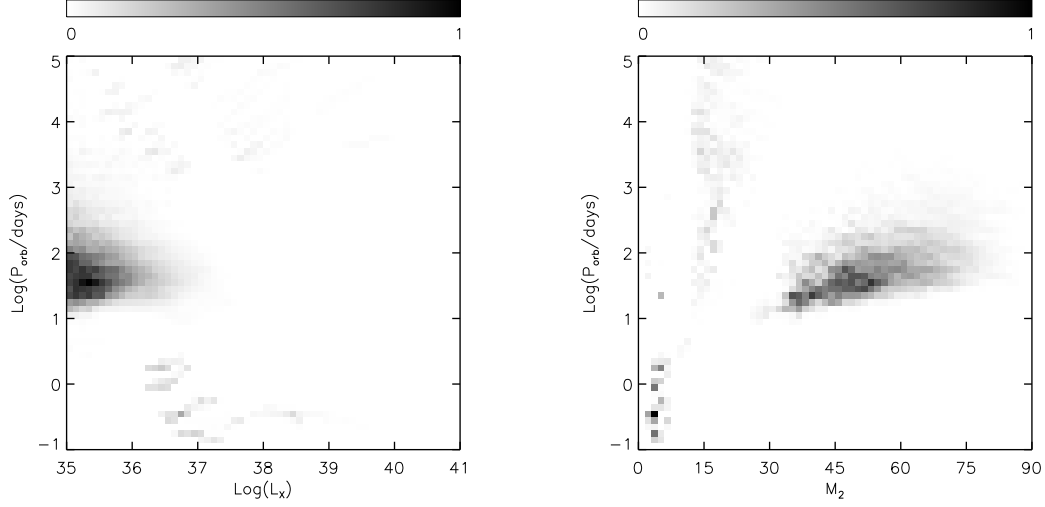


Fig. 2.— The current orbital period $P_{\text{orb}} - L_X$ (left) and $P_{\text{orb}} - M_2$ (right) distributions in model M1.

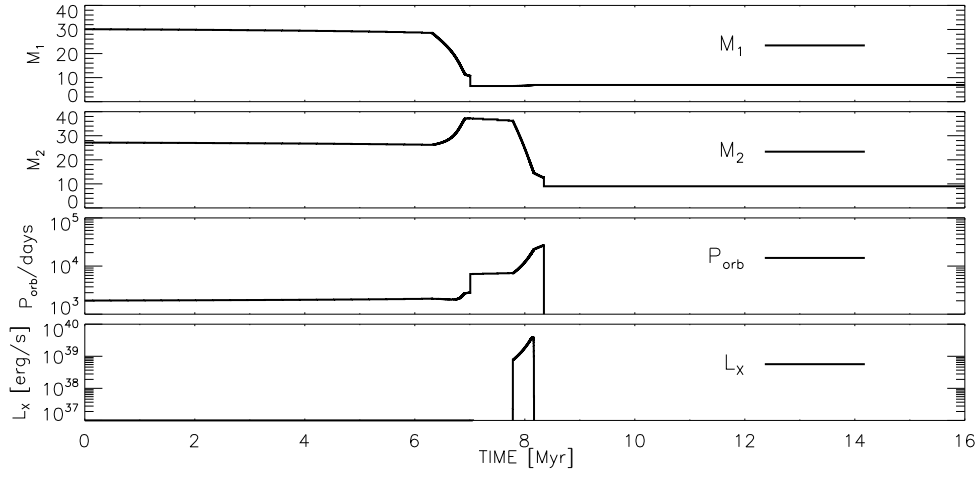


Fig. 3.— The evolution of M_1 , M_2 , P_{orb} , and L_X for an example of bright BH-SG HMXBs in model M1.

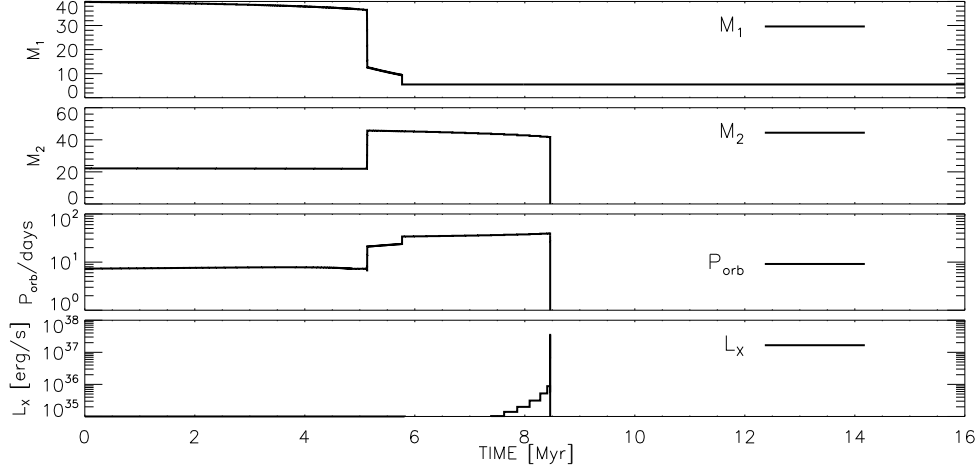


Fig. 4.— The evolution of M_1 , M_2 , P_{orb} , and L_X for an example of low luminosity BH-MS HMXBs in model M1.

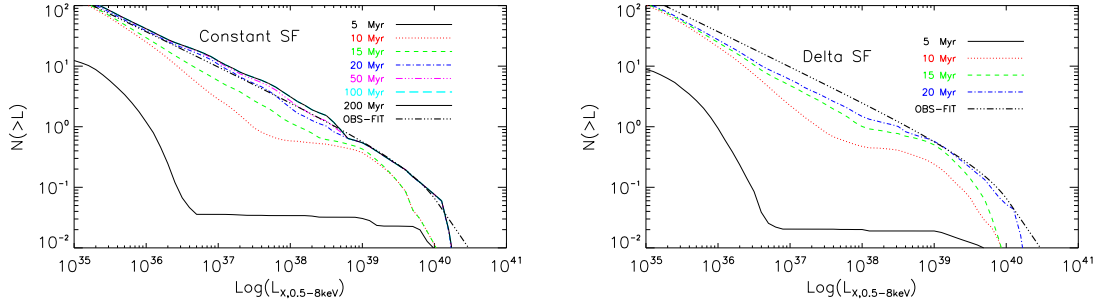


Fig. 5.— The evolution of XLF in model M1. *Left* panel: We adopted a constant star formation for 5 Myr (thick solid line), 10 Myr (dotted line), 15 Myr (short-dashed line), 20 Myr (dash-dotted line), 50 Myr (dash-dot-dotted), 100 Myr (long-dashed line), and 200 Myr (thin solid line), respectively. *Right* panel: A δ -function like star formation episode is adopted. Here the star formation history is set as 20 Myr, with peak SFR = $1 M_{\odot}/\text{yr}$ in the middle. The solid, dotted, dashed and dash-dotted lines represent the XLFs at the age of 5 Myr, 10 Myr, 15 Myr and 20 Myr since the beginning of the star formation, respectively. The thick dash-dot-dotted line represents the observed average XLF.

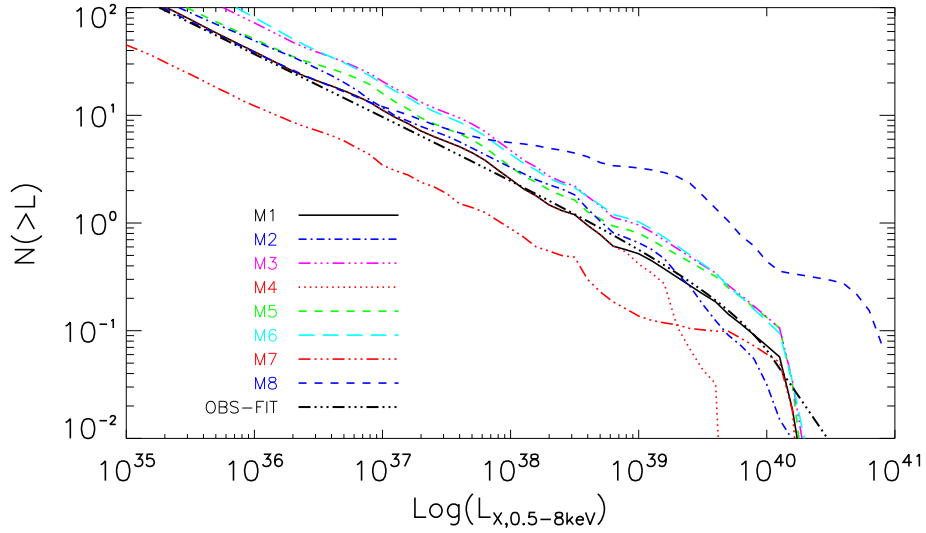


Fig. 6.— Comparisons of the simulated and observed average (labeled as “OBS-FIT”, thick dash-dot-dotted line) XLFs. Compared to the basic model M1 (solid line), in M2 (dash-dotted line) the CE parameter α_{CE} is increased to a value 1.0, in M3 (dash-dot-dotted line), the binary fraction f is set as 0.8. In M4 (dotted line), the factor for super-Eddington accretion rate is decreased by a factor of 20. We take an atypical distributions of mass ratio in M5 (short-dashed line) and a flatter IMF in M6 (long-dashed line), respectively. In M7 (dash-dot-dotted line), the dispersion of kick speed is increased to $\sigma_{\text{kick}} = 265 \text{ km s}^{-1}$. We reduce the standard wind mass loss rate by a factor of 2 in M8 (short-dashed line).

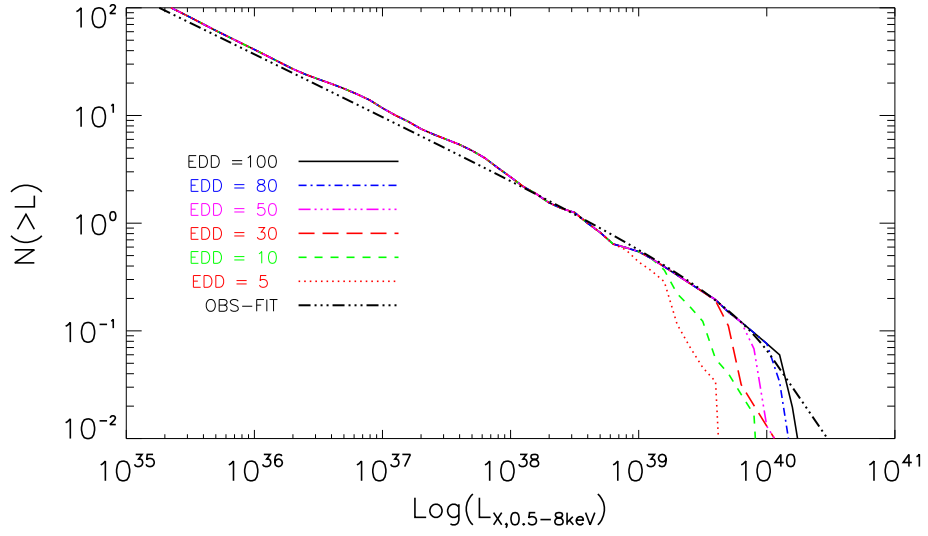


Fig. 7.— Comparisons of the simulated XLFs with super-Eddington factors (η_{Edd}) adopted as 100 (the basic model, M1, solid line), 80 (dash-dotted line), 50 (dash-dot-dotted line), 30 (long-dashed line), 10 (short-dashed line), and 5 (dotted line), respectively. The thick dash-dot-dotted line represents the observed average XLF.

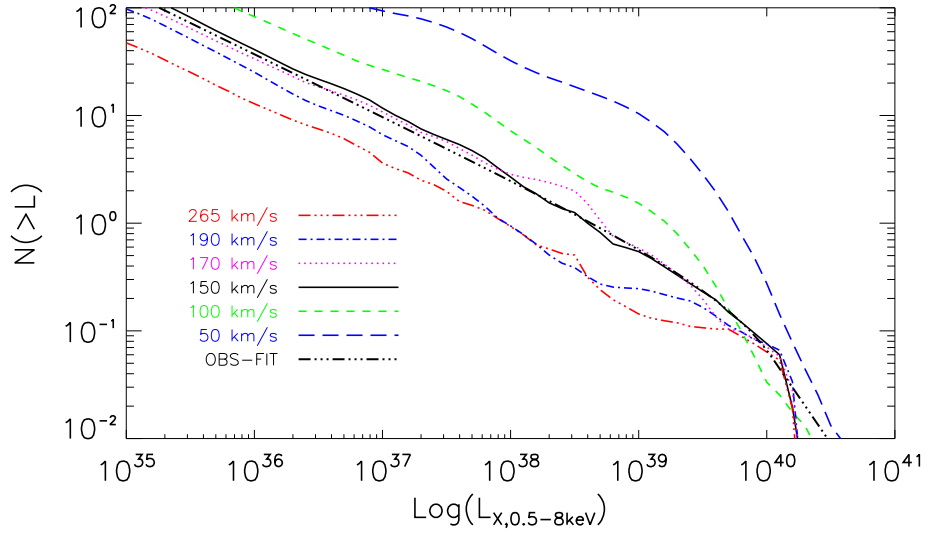


Fig. 8.— Comparisons of the simulated XLFs with the dispersion of kick velocity (σ_{kick}) adopted as 265 (dash-dot-dotted line), 190 (dash-dotted line), 170 (dotted line), 150 (the basic model, M1, solid line), 100 (short-dashed line) and 50 (long-dashed line), respectively. The thick dash-dot-dotted line represents the observed average XLF.

Table 2: Fitting formula coefficients of CE criterion. Here q is the initial mass ratio, a_n ($n=0-5$) is the coefficient of the binomial. Note that a blank entry in the table implies a zero value.

q	a_0	a_1	a_2	a_3	a_4	a_5
2	-7.55E-1	4.577E-1	-2.06E-2	3.88E-4	-2.57E-6	
2.5	-1.955E+0	1.026E+0	-4.937E-2	9.36E-4	-6.14E-6	
3	-3.278E+0	1.565E+0	-6.628E-2	1.07E-3	-6.01E-6	
3.5	2.4E-1	4.05E-1	1.299E-1	6.44E-3	1.06E-4	-5.75E-7
4	-1.341E+1	5.232E+0	-1.496E-1	1.144E-3		
4.5	1.143E+2	-1.997E+0	4.168E-3			
5	1.612E+2	-2.44E+0	-6.85E-4			
6	1.911E+2	1.558E+1	-6.27E-1	5.35E+3		
8	5.8938E+3	-1.9817E+2	1.6907E+0			
10	3.96712E+4	-1.38555E+3	1.2168E+1			
12	7.86627E+4	-2.64895E+3	2.2478E+1			
ALL	8.9493E+0	-2.7841E+3	6.285E-1	2.7E-3		